J Mater Sci: Mater Med (2010) 21:741–751
DOI 10.1007/s10856-009-3871-5

Construction of collagen II/hyaluronate/chondroitin-6-sulfate tri-copolymer scaffold for nucleus pulposus tissue engineering and preliminary analysis of its physico-chemical properties and biocompatibility

Chang-qing Li · Bo Huang · Gang Luo · Chuan-zhi Zhang · Ying Zhuang · Yue Zhou

Received: 22 June 2009 / Accepted: 9 September 2009 / Published online: 18 September 2009

Abstract To construct a novel scaffold for nucleus pulposus (NP) tissue engineering, The porous type II collagen (CII)/hyaluronate (HyA)–chondroitin-6-sulfate (6-CS) scaffold was prepared using 1-ethyl-3-(3-dimethylaminopropyl)-carbodiimide (EDC) and *N*-hydroxysuccinimide (NHS) cross-linking system. The physico-chemical properties and biocompatibility of CII/HyA–CS scaffolds were evaluated. The results suggested CII/HyA–CS scaffolds have a highly porous structure (porosity: 94.8 ± 1.5%), high water-binding capacity (79.2 ± 2.8%) and significantly improved mechanical stability by EDC/NHS crosslinking (denaturation temperature: 74.6 ± 1.8 and 58.1 ± 2.6°C, respectively, for the crosslinked scaffolds and the non-crosslinked; collagenase degradation rate: 39.5 ± 3.4 and 63.5 ± 2.0%, respectively, for the crosslinked scaffolds and the non-crosslinked). The CII/HyA–CS scaffolds also showed satisfactory cytocompatibility and histocompatibility as well as low immunogenicity. These results indicate CII/HyA–CS scaffolds may be an alternative material for NP tissue engineering due to the similarity of its composition and physico-chemical properties to those of the extracellular matrices (ECM) of native NP.

Chang-qing Li and Bo Huang are co-first authors. Both authors contributed equally to this work.

C. Li · B. Huang · G. Luo · C. Zhang · Y. Zhuang · Y. Zhou (✉)
Department of Orthopedics, Xinqiao Hospital, Third Military Medical University, Chongqing 400037, People's Republic of China
e-mail: happyzhou@vip.163.com

1 Introduction

Low back pain (LBP) is a very frequently encountered disorder, the incidence of which is second only to upper respiratory infections. In addition, LBP is also the predominant cause of disability [1]. Disc degenerative diseases (DDD) are generally thought to be the main cause of LBP [2–4]. DDD are caused by abnormal mechanical loading, genetic predisposition, reduced cell activity, or any combination of the three, inducing changes in the matrix composition and resulting in the deterioration of its biomechanical properties [5, 6].

Current therapies for DDD range from conservative management to invasive procedures such as discectomy, spinal fusion, total disc replacement, or NP replacement [7]. Conservative management strategies include bed rest (although this is no longer recommended), analgesia, muscle relaxants, corticosteroids or local anesthetics and manipulation therapies, while all of which are mainly palliative. Surgical treatments, such as discectomy and spinal fusion, produce symptomatic relief by removing the disc tissue or sacrificing the mobility of spinal segments rather than repairing the degenerated discs. Although artificial disc replacement surgery has been demonstrated a promising future, many complications and shortcomings associated with this technology still need to be overcome [8].

None of the surgical treatments for DDD are currently applied to deal with the inherent loss of functional native disc tissue; therefore, biological implants consistent with structure and function of intervertebral disc (IVD) and/or NP may be ideal candidates for reconstituting the degenerated discs and therefore treating DDD. With the rapid development of tissue engineering in recent years, IVD tissue engineering has provided a possibility for recovering the function of the IVD with in vitro development of

functional tissue unit for implantation into the body. The aim of IVD tissue engineering is to induce regeneration of the degenerated disk in situ via biological manipulation. Among the three anatomical elements of IVD (the annulus fibrosus, the NP, and the endplate), the gelatinous NP comprises randomly organized collagen fibers, radially arranged elastin fibers and a highly hydrated aggrecan containing gel [9, 10]. The highly hydrated proteoglycans in the NP are essential to maintain the osmotic pressure and therefore have a major effect on the load bearing properties of the disc [11]. In addition, as DDD is believed to originate from a gradual loss of proteoglycans and water content in NP [12], most tissue engineering studies are focused on treatment of degenerated NP.

Among the three principal components of tissue engineering (cells, scaffolds, and signals), the scaffold acts as a delivery vehicle, providing cells with temporary protection from unfavorable local implantation milieu. In addition, it should also create an environment that favors cell adhesion, proliferation, related gene expression and synthesis of new functional tissues [13]. At present, although an extensive body of literature exists on NP tissue engineering scaffolds, few studies have mentioned specific scaffold materials that imitate the natural environmental condition of native NP [14]. As the main function of a biological scaffold is to emulate the biological environment of the local tissue, a scaffold for the tissue engineered NP must therefore simultaneously provide the three principal extracellular matrix components of native NP: CII, HyA and 6-CS. According to the principal described above, we have constructed a novel scaffold composed of CII, HyA and 6-CS using EDC/NHC as a crosslinking agent and performed a preliminary analysis of its physico-chemical properties and biocompatibility.

2 Materials and methods

2.1 Fabrication of CII/HyA–CS scaffolds

2.1.1 Preparation of CII/HyA sponge

CII (164.2 mg, from porcine cartilage; Chuanger Co, China) was completely dissolved into 0.01 M hydrogen chloride (HCL) solution (pH 2–3) by stirring (300 rpm) at 4°C to a final concentration of 1.25% (w/v). The pH of the CII solution was adjusted to about 1–2. A solution of HyA (1.25%, w/v) was prepared by dissolving HyA (MW: 0.8–2.0 $\times$ 10^6; H7630; Sigma Chemical Co.) in distilled water and cooled to 4°C. Then, the pre-cooled HyA solution was dripped at a speed of 0.5 ml/min into the prepared CII solution to a final ratio of 1–9 (v:v; HyA to CII), which mimics the HyA to CII ratio in the native NP tissue, and stirred (300 rpm) at 4°C for 4 h. The mixed solution was centrifuged (3000 rpm, 15 min) at 4°C to remove air bubbles and then poured gently into a 50-mm culture dish and frozen at −80°C overnight. The CII/HyA sponge was constructed by lyophilizing the mixed solution for 24 h.

2.1.2 Detection of polyion complex (PIC) formation

A total of 100 µl of CII solution (pH 1–2) and 100 µl of CII/HyA solution (pH 1–2) were added to two separate cuvettes. The transmittance of HCL solution at pH 1–2 was used as the blank control, and the transmittances of the CII solution and CII/HyA solution at 500 nm were measured, respectively, by a Beckman 800U spectrophotometer. Six specimens of each kind of solution were detected.

2.1.3 Crosslinking of CII/HyA–CS scaffolds

50 mg of dried CII/HyA sponge was immersed in 20 ml of 40% ethanol containing 50 mM 2-morpholino-ethanesulfonic acid (MES, Fluka Chemie AG, Buchs, Switzerland) (pH 5.5) for 30 min at room temperature, and then incubated in 20 ml of 40% ethanol containing 50 mM MES, 24 mM EDC (Fluka Chemie AG), 5 mM NHS Fluka Chemie AG) and 2% 6-CS (w/v) (Sigma Chemical Co.) for 24 h at room temperature (RT) for crosslinking. The processed scaffold was washed twice with 0.1 M Na_2HPO_4 (pH 9.1) for 1 h, twice with 1 M NaCl for 2 h, six times with 2 M NaCl for 24 h and finally ten times with ultrapure water for 2 h. The scaffold was then lyophilized for 24 h. The dried CII/HyA–CS scaffold was cut into 2 mm-thick discs with a diameter of 10 mm, then sterilized by soaking in 70% ethanol overnight and washed with phosphate-buffered saline (PBS) five times before cell seeding.

2.2 Determination of the physico-chemical and morphologic characteristics of the CII/HyA–CS scaffold

2.2.1 Extraction of GAG

Six of the CII/HyA–CS scaffolds (each weight = 10 mg) were cut into small pieces and put into 1.5 ml Eppendorf tubes respectively. A total of 1.5 ml of 0.1 M NaOH was added to each tube to prepare the homogenate solution, and 0.1 M HCl was added to neutralize the solution to pH 7.4. Then, 1 ml of 1 mg/ml tryptase was added. After incubation at 37°C for 24 h, 60% trichloroacetic acid (TCA) (w/v) was added to a final concentration of 10% (w/v) and incubated at RT for 24 h. After centrifugation, the supernatant, which was protein free, was collected and 4 volumes of 100% ethanol was added. The mixture was then centrifuged and the supernatant discarded. The precipitates

were resolved in 1 ml of distilled water and the content and composition of GAG were determined in the following experiment.

2.2.2 Determination of GAG contents

A total of 1.5 ml of alcian blue dye was added to each 0.1 ml solution extracted in the foregoing step and mixed. Ten minutes later, the absorbances of the solutions were measured at 480 nm on a microplate absorbance reader (VARIO SKAN FLASH, Thermo Electron Corporation, USA) and compared with the linear standard curve obtained from 100 to 200 μg/ml 6-CS standard.

2.2.3 Compositional analysis of GAG

A total of 5 μl of HyA, 6-CS standard preparation, and 10 μl of GAG solution specimen ($n = 6$) were resolved on 10% sodium dodecyl sulfate-polyacrylamide gels. Immediately after electrophoresis, gels were fixed and stained with alcian blue and silver nitrate [15]. The grey scales for HyA and CS components were obtained by scanning the gel image (Chemiimage 5500) and the percentage of each component was calculated by comparing the gray scale of each component with that of total GAG from the same sample.

2.2.4 Observation of the microstructure of scaffold materials

Scaffolds were fixed in neutral buffered formalin and embedded in paraffin. The embedded samples were sectioned with a microtome at a thickness of 2 μm, and then stained with hematoxylin and eosin (H&E) for histological examination and toluidine blue for glycosaminoglycan examination. The porous structure was observed using an Olympus optical microscope. For scanning electron microscopy (SEM), the scaffolds or the cell/scaffold hybrids at each time point were fixed in PBS (pH 7.4, 4°C) for at least 24 h. Then, the samples were dehydrated in a graded series of ethanol solutions, air-dried, sputter-coated with gold and examined using a HITACHI-3400N scanning electron microscope.

2.2.5 Porosity testing

The pore diameter of the scaffold was characterized using the HITACHI-3400 N scanning electron microscope with an image analyzing system (Escan 4000, Bum-Mi Universe Co., Ltd., Ansan, Korea). The image analysis program was used to calculate the mean pore diameter, and at least 50 pores were assessed.

The porosity was determined with an ethanol displacement method reported by Zhang et al. [16]. One scaffold sample was immersed in a graduated cylinder containing a known volume (V_1) of ethanol. The sample was kept in the ethanol for 5 min, followed by a series of brief evacuation–repressurization cycles that were conducted to force the ethanol into the pores of the scaffold. Cycling was continued until no air bubbles emerged from the scaffold. The total volume of ethanol plus the ethanol-impregnated scaffold was then recorded as V_2. The volume difference ($V_2 - V_1$) was the volume of the skeleton of the scaffold. The ethanol-impregnated scaffold was removed from the cylinder, and then the residual ethanol volume was recorded as V_3. The quantity of ethanol retained in the scaffold ($V_1 - V_3$) was defined as the void volume of the scaffold; thus, the total volume of the scaffold was $V = (V_2 - V_1) + (V_1 - V_3) = V_2 - V_3$. The porosity of the scaffold, ε, was calculated by $\varepsilon = [(V_1 - V_3)/(V_2 - V_3)] \times 100\%$. Six scaffold samples were examined in this test.

2.2.6 Determination of water-binding capacity

5 mg (dry weight, W_d) of crosslinked CII/HyA–CS scaffold ($n = 6$) was incubated with 3 ml PBS (pH 7.2) at 20°C for 1 h, removed from the PBS, placed on a glass plate at a 60° angle from horizontal for 2 min and wiped with tissue paper. The weight of the wet scaffold (W_w) was then recorded. The water-binding capacity was determined by calculating the water content: $[(W_w - W_d)/W_w] \times 100\%$ [17].

2.2.7 Denaturation temperature

Two milligrams of scaffold in 50 μl PBS (pH 7.2) was incubated in a thermal denaturation analyzer (Perkin-Elmer DSC-7) at 20°C for 2 h. Then the temperature was increased to 90°C at a rate of 5°C/min and the denaturation temperatures of the crosslinked scaffolds ($n = 6$) and the non-crosslinked scaffolds ($n = 6$) were recorded separately and compared [18].

2.2.8 In vitro degradation by collagenase

Scaffolds ($n = 6$) were accurately weighted and immersed in 1 ml of 0.1 M Tris–HCl containing 0.05 M $CaCl_2$ (pH 7.4) and incubated at 37°C for 1 h. Then, 1 ml of 0.1 M Tris–HCl containing 200 U collagenase II (Sigma) was added. A total of 0.2 ml of 0.25 M ethylenediamine tetraacetic acid (EDTA) was added to terminate the digestion 24 h later. The samples were centrifugated ($5000 \times g$, 15 min, 4°C). The precipitates were washed three times in distilled water (4°C) and finally lyophilized. Scaffold degradation was determined from the weight of residual scaffold, and expressed as a percentage of the original

weight. The degradation rates of the non-crosslinked scaffolds ($n = 6$) were calculated for comparative analysis.

2.3 Evaluation of the cytocompatibility of CII/HyA–CS scaffolds with NP cells

2.3.1 Rabbit NP cell isolation and cocultivation with CII/HyA–CS scaffolds

All animal experiments were conducted in conformity with the "Guiding Principles for Research Involving Animals and Human Beings" as adopted by The American Physiological Society and with approval by Institutional Review Board (Third Military Medical University, Chongqing, PR China). New Zealand White rabbits, approximately 3 weeks old and 1 kg in weight, were used for the study. Rabbits were sacrificed by an overdose of Nembutal (100 mg/kg, Veterinary Laboratory Inc., Lenexa, KS). Thoracic and lumbar spines were obtained under aseptic conditions within 1 h after death. The annulus fibrosus was exposed, and the gelatinous NP was harvested. Samples were collected from the central portion of the NP to ensure that no fibrous tissue contamination occurred. The obtained NP tissues were washed for three times with 0.1 M PBS containing 100 U/ml each of penicillin (GIBCO) and streptomycin (GIBCO) and then treated with 0.25% collagenase from clostridium histolyticum (Sigma Co.) at 37°C for approximately 30–35 min. The digested tissues were passed through a cell strainer (Becton–Dickinson Labware, Franklin Lakes, NJ) with a pore size of 100 μm. Cells were recovered by centrifugation at 1000 rpm for 10 min. The isolated cells were then washed three times with DMEM/F12 supplemented with 15% heat-inactivated fetal bovine serum (GIBCO), 25 mg/ml L-ascorbic acid (Sigma Co.) and 50 U/ml of penicillin and streptomycin. The cell yield was assessed using a hemocytometer, and the viability was determined by a trypan blue exclusion method. Approximately 2×10^6 cells were isolated per rabbit. The cells were expanded in a monolayer culture in DMEM/F12 supplemented with 15% heat-inactivated fetal bovine serum, 25 mg/ml L-ascorbic acid and 50 U/ml of penicillin and streptomycin at 37°C in an atmosphere of 5% CO_2 and 95% air. The passage 1 (P1) cells were used for seeding into the scaffolds.

The sterilized CII/HyA–CS scaffolds (2 mm-thick, 10 mm in diameter) were placed in 6-well plate wells, and then 100 μl of cell suspension containing 1×10^5 NP cells was completely seeded into each scaffold. The cell-containing scaffolds were incubated at 37°C, 5% CO_2 and 95% humidity for 2 h, then the culture medium was supplemented slowly for further culture. For monolayer culture group, 6-well plates were directly plated by NP cells at a density of 1×10^5 cells/well. Culture medium was changed every 2 days for both groups. Cultures were terminated after 1, 3, 5 and 7 days, respectively.

2.3.2 DNA synthesis

After 7 days of culture, cells of each group were fed for the last 24 h with DMEM/F12 containing [^{3}H]-thymidine (Amersham, Piscataway, NJ) at concentration of 2 μCi/ml per well for 24 h. Then, monolayer cultured cells and cell/scaffold hybrids were digested respectively in 1 ml of papain solution (20 mg/ml in 50 mM EDTA, 5 mM L-cysteine) for 18 h at 55°C. A 100 μl aliquot of each sample was collected and preserved for DNA content measurement. A total of 2 ml of 10% TCA was then added to each well. The mixtures were centrifuged (3000 rpm for 10 min) and the supernatants were removed. This procedure was repeated for five times, and the TCA-insoluble material was collected and washed with 70% ethanol. The insoluble material was then treated overnight with 1 ml of solvent (Solvable, Packard, Meriden, USA) at 45°C and 10 ml of liquid scintillation cocktail (Atomlight, Packard, Meriden, USA) was added (Beckman LS4800, Fullerton, USA). The radioactivity of each sample, in disintegrations per minute (DPM), was divided by their DNA content, quantified as described below. The radioactivity of each sample was expressed as DPM per μg of DNA. Five samples of each group were evaluated.

2.3.3 Determination of DNA content

To measure the DNA content of each group on day 1, 3, 5, and 7, respectively, after seeding, monolayer cultured cells and cell/scaffold hybrids were digested respectively in 1 ml of papain solution (20 mg/ml in 50 mM EDTA, 5 mM L-cysteine) for 18 h at 55°C. A 100 μl aliquot was mixed with 1 ml of bisbenzimidazole fluorescent dye/buffer (Hoechst 33258, Molecular Probes, Eugene, OR), and then 200 μl of each mixture was pipetted into a 96-well microtiter plate and evaluated for emission at 458 nm excited at 365 nm by the microplate absorbance reader (VARIO SKAN FLASH, Thermo Electron Corporation, USA). A standard curve was constructed from known concentrations of calf thymus DNA (Sigma, St. Louis, MO). Five samples of each group were evaluated at each time point.

2.4 Detection of the histocompatibility and immunogenicity of CII/HyA–CS scaffolds

2.4.1 Surgical implantation of scaffolds

One hundred and five 2 month-old male Sprague–Dawley (SD) rats were randomly divided into three groups, among

which the untreated group, the sham-operated group and the implanted groups contained 35 animals each. Anesthesia was induced by intraperitoneal injection of Nembutal (30 mg/kg); after shaving and disinfection, a small transverse incision was made in the skin of the dorsal median zone, and a subcutaneous pocket was made. In the implanted group, a square of CII/HyA–CS scaffold (1 cm × 1 cm, sterilized) was inserted into the pocket and the incision was closed, whereas in the sham-operated group the incisions were closed directly after subcutaneous pockets were made. Nothing was done to the untreated group. For analysis by enzyme linked immunosorbent assay (ELISA), blood was obtained from each group at various time points (1, 3, 7, 14, 28, 56, and 84 days) by cardiac puncture and the sera were stored at −80°C until use. Meanwhile on day 1, 3, 7, 14, 28, and 84, the implants with surrounding tissues and the underlying muscles were carefully dissected from the subcutaneous sites and fixed in 2% (v/v) glutaraldehyde in 0.1 M phosphate buffer (pH 7.4) for at least 24 h at 4°C.

2.4.2 Histological analysis of implants

After fixation, the explants were dehydrated in graded alcohol, cleared in butanol and embedded in paraffin wax. Four micron sections were cut and mounted onto positively charged slides. Adherence was ensured by heating the slides at 55°C. Staining was performed with H&E for histological examination.

2.4.3 Determination of antibodies against porcine CII

Circulating antibodies against native porcine CII were measured using the rat anti-porcine CII antibody detection kit (Chondrex), as described previously. Rat sera diluted from 1:10 to 1:1000 were allowed to react with porcine CII (from porcine cartilage; Chuanger Co, China) coated microplates. The sensitivity of the test was enhanced by addition of rabbit IgG directed against rat IgG, and OPD-carbamide H_2O_2 was added to detect collagen-antibody complexes. The absorbance at 490 nm was measured using a microplate absorbance reader (VARIO SKAN FLASH, Thermo Electron Corporation, USA). A nonspecific binding control using PBS–bovine serum albumin instead of serum was set up to exclude nonspecific binding. Rat sera from the untreated group were used as negative controls. Sera from the sham-operated rats were analyzed to exclude any effects from the operation. OD values were automatically converted into contents (units/ml) by the microplate absorbance reader.

2.5 Statistical analysis

Statistical analysis was performed using SPSS software (version 13.0). The data were expressed as mean ± standard deviation. Comparison of group means was performed using Student's *t*-test. A one-way ANOVA was used to compare the expression level of anti-porcine CII antibodies among the implanted group, untreated group and sham-operated group at various time points. *P*-values of less than 0.05 were considered significant.

3 Results

3.1 Characterization of CII/HyA–CS scaffolds

3.1.1 Formation of PIC

There was no significant difference ($P > 0.05$) when comparing the transmittance of CII/HyA solution (98.3 ± 1.3%) with that of CII solution (98.4 ± 0.9%), which indicates that almost no PIC was formed at pH 1–2 when HyA solution was added (Fig. 1).

3.1.2 GAG content and components in the scaffold materials

The mean content of GAG in the CII/HyA–CS scaffold materials was 222.1 ± 19.4 mg/g including 37.5% ± 1.8% HyA and 62.5% ± 1.8% CS.

3.1.3 Microscopic observation of the scaffold

CII/HyA–CS scaffolds were acidophilic with a neatly arranged porous structure (Fig. 2a). The scaffold was stained purple by toluidine blue, which indicated that sulfated GAGs were attached to the collagens (Fig. 2b).

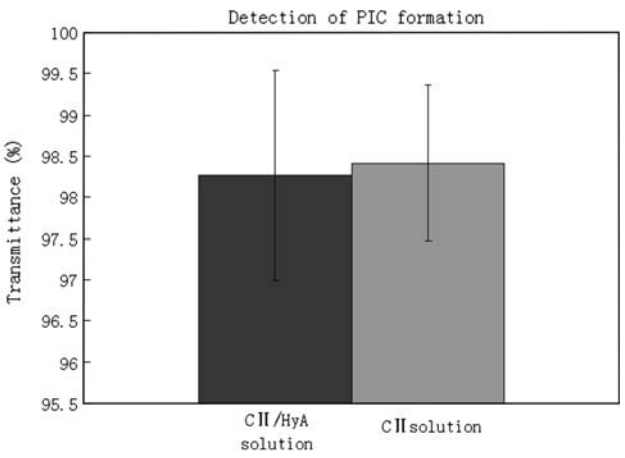

Fig. 1 Detection of PIC formation. No significant difference ($P > 0.05$) was observed between the transmittance of the CII/HyA solution (98.3 ± 1.3%) and that of the CII solution (98.4 ± 0.9%) when the pH value was maintained at 1–2, which indicates that almost no PIC was formed when HyA solution was added

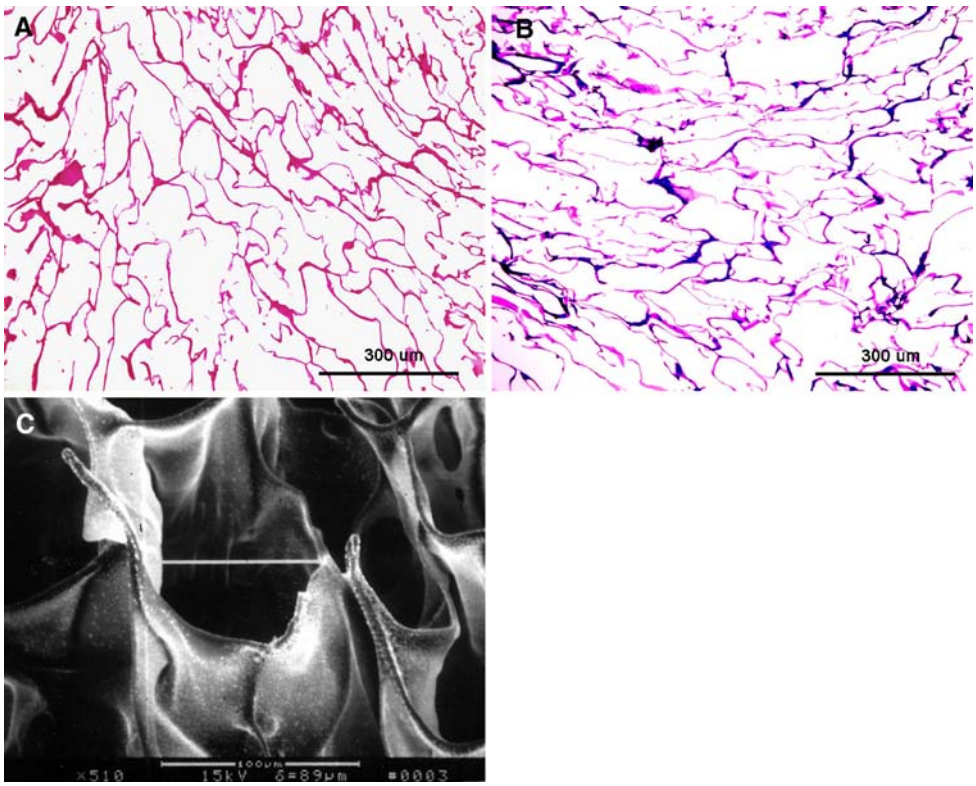

Fig. 2 Microscopic observation of the scaffold. **a** Porous structure of the scaffold (H&E, ×100); **b** GAG-attached scaffold (toluidine blue, ×100); **c** The ultrastructure of the scaffold (SEM, ×510)

The scaffold had an interconnected pore structure with a mean pore size of 110 ± 21 μm (Fig. 2c).

3.1.4 Porosity

The porosity of the scaffold ranged from 93.3 to 96.3%, with a mean value of 94.8 ± 1.5% (Table 1).

3.1.5 Water-binding capacity

The water-binding capacity of the scaffold ranged from 76.4 to 82.0%, with a mean value of 79.2 ± 2.8% (Table 1).

3.1.6 Denaturation temperature

The denaturation temperature of the crosslinked scaffolds was 74.6 ± 1.8°C, which was significantly higher than 58.1 ± 2.6°C for the non-crosslinked scaffolds ($P < 0.01$) (Table 1).

3.1.7 Collagenase degradation rate

The collagenase degradation rate of the crosslinked scaffolds was 39.5 ± 3.4%, while that of the non-crosslinked scaffolds was 63.5 ± 2.0%. The significant difference ($P < 0.01$) indicated that the crosslinked scaffold materials had better resistance to collagenase induced degradation (Table 1).

3.2 Cytocompatibility of CII/HyA–CS scaffolds with NP cells

3.2.1 Cell proliferation

DNA synthesis as measured by uptake of [^{3}H]-thymidine measurement showed no significant difference ($P > 0.05$) between cell/scaffold hybrids (13310.68 ± 1536.17 DPM/μg DNA) and monolayer cultured cells (12622.40 ± 1268.83 DPM/μg DNA) on day 7 of culture (Fig. 3a). DNA content measurement demonstrated similar results. No significant differences ($P > 0.05$) in DNA content were noticed among cell/scaffold hybrids and monolayer cultured cells at each time point. (On day 1, monolayer: 771.27 ± 53.80 versus hybrids: 748.31 ± 21.51; on day 3, monolayer: 1203.63 ± 126.92 versus hybrids: 1242.48 ± 176.35; on day 5, monolayer: 1467.21 ± 94.10 versus hybrids: 1418.91 ± 162.75; on day 7, monolayer: 1561.02 ± 79.85 versus hybrids: 1571.48 ± 140.50; all values were expressed as nanogram, Fig. 3b).

3.2.2 SEM for cell/scaffold hybrids

An SEM photograph taken 2 h after cell seeding showed that NP cells with spherical morphology had attached to the scaffold (Fig. 4a). After 7 days of culture, initiation of new pericellular matrix production by NP cells could be seen

Table 1 Characterization of the scaffold materials ($n = 6$)

	Porosity (%)	Water-binding capacity (%)	Denaturation temperature (°C)	Collagenase degradation (%)
Crosslinked scaffolds	94.8 ± 1.5	79.2 ± 2.8	74.6 ± 1.8*	39.5 ± 3.4*
Non-crosslinked scaffolds	–	–	58.1 ± 2.6	63.5 ± 2.0

* $P < 0.01$, vs. non-crosslinked scaffolds

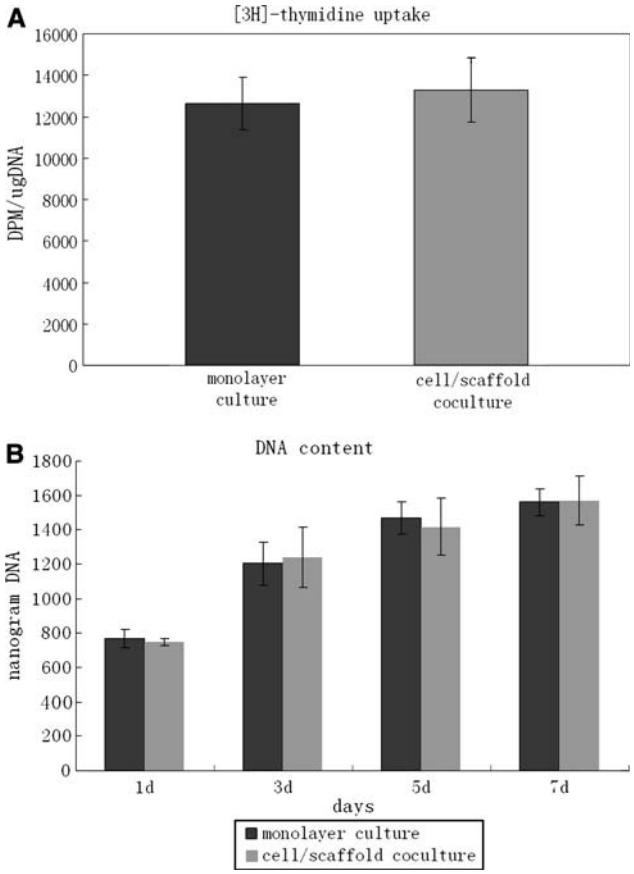

Fig. 3 Cell proliferation assays. **a** DNA synthesis after 7 days of culture showed no significant difference between the monolayer culture group and the cell/scaffold coculture group ($P > 0.05$). **b** DNA content analysis also showed no significant difference between the two groups at all the time points ($P > 0.05$)

and the cellular shape could still be recognized through pericellular matrix (Fig. 4b).

3.3 Histocompatibility and immunogenicity of CII/HyA–CS scaffolds

3.3.1 In vivo degradation and tissue reactions

One day after implantation, the scaffold had been infiltrated by some lymphocytes and neutrophils, which was typical of a normal foreign-body reaction. These inflammatory cells were present at the peripheral and internal space of the implant (Fig. 5a). After 3 days, the number of infiltrated inflammatory cells increased within the implant and in the surrounding connective tissue (Fig. 5b). On day 7, the amount of inflammatory cells had decreased with the scaffold partially degraded (Fig. 5c). By 14 days, fibroblasts had arrived from surrounding granulation tissues; degradation of the scaffold continued (Fig. 5d). On day 28, the implant was surrounded and partially replaced by granulation tissues filled with fibroblasts. Some blood vessels had colonized the granulation tissues (Fig. 5e). Between 28 and 84 days, the implant had been further degraded. Almost all traces of the implanted scaffold had disappeared and the scaffold had been totally replaced by the vascularized granulation tissues in the end (Fig. 5f).

3.3.2 Detection of antibodies to porcine CII

At the various time points, there was no significant variation ($P > 0.05$) in the expression level of anti-porcine CII antibodies when compared among the implanted group, untreated group and sham-operated group. Therefore, almost no antibodies against porcine CII were detected in the sera of the implanted rats (Table 2).

4 Discussions

Tissue engineering research has been carried out for decades. Tissue-engineered skin has been approved by the FDA for clinical treatment in the USA, and tissue-engineered cartilage and bone have been experimentally applied in clinical treatment in some other countries. However, research on tissue-engineered IVD is still in its primary stage. Most of the scaffold materials used in tissue-engineered NP are collagen I (CI) [19, 20] or other macromolecules such as poly-(D,L-lactide) [21], calcium polyphosphate substrate [22], alginate [23, 24], small intestine submucosa (SIS) [25], HyA [26], chitosan [27] and a mixture of gelatin, 6-CS, and HyA [28], most of which are derived primarily from tissue-engineered cartilage or bone. Under physiological conditions, CII, but not CI, is the main component of the ECM of native NP tissue. CII is different from CI in regard to structure and hydrophilicity. Some work on injectable cell-seeded scaffolds using atelocollagen II gel have been reported [29, 30]. Nevertheless, Gruber and his colleagues compared the biological function of collagen sponge, collagen gel, agarose, alginate, or fibrin gel formulations. They confirmed collagen sponges

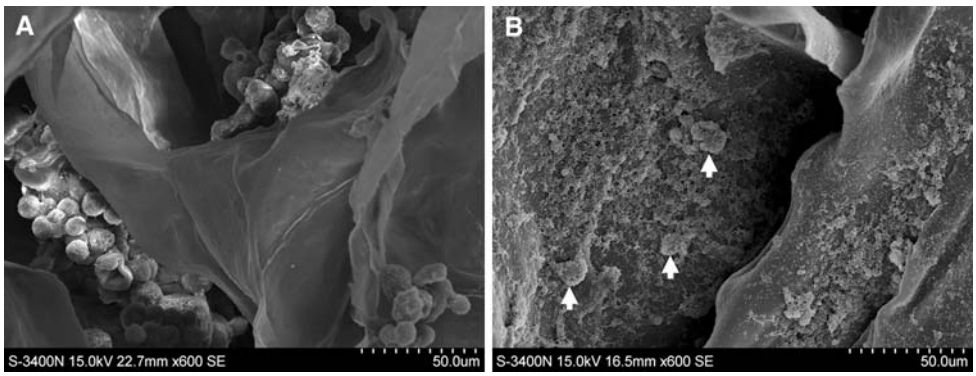

Fig. 4 SEM of the cell/scaffold hybrids. **a** SEM photograph of the surface of the CII/HyA–CS scaffold 2 h after seeding with NP cells. Note the attached NP cells with spherical morphology (SEM, ×500). **b** SEM photograph of the surface of the CII/HyA–CS scaffold 7 days after seeding. Note that the NP cells (*arrows*) are covered by newly synthesized pericellular matrices (SEM, ×500)

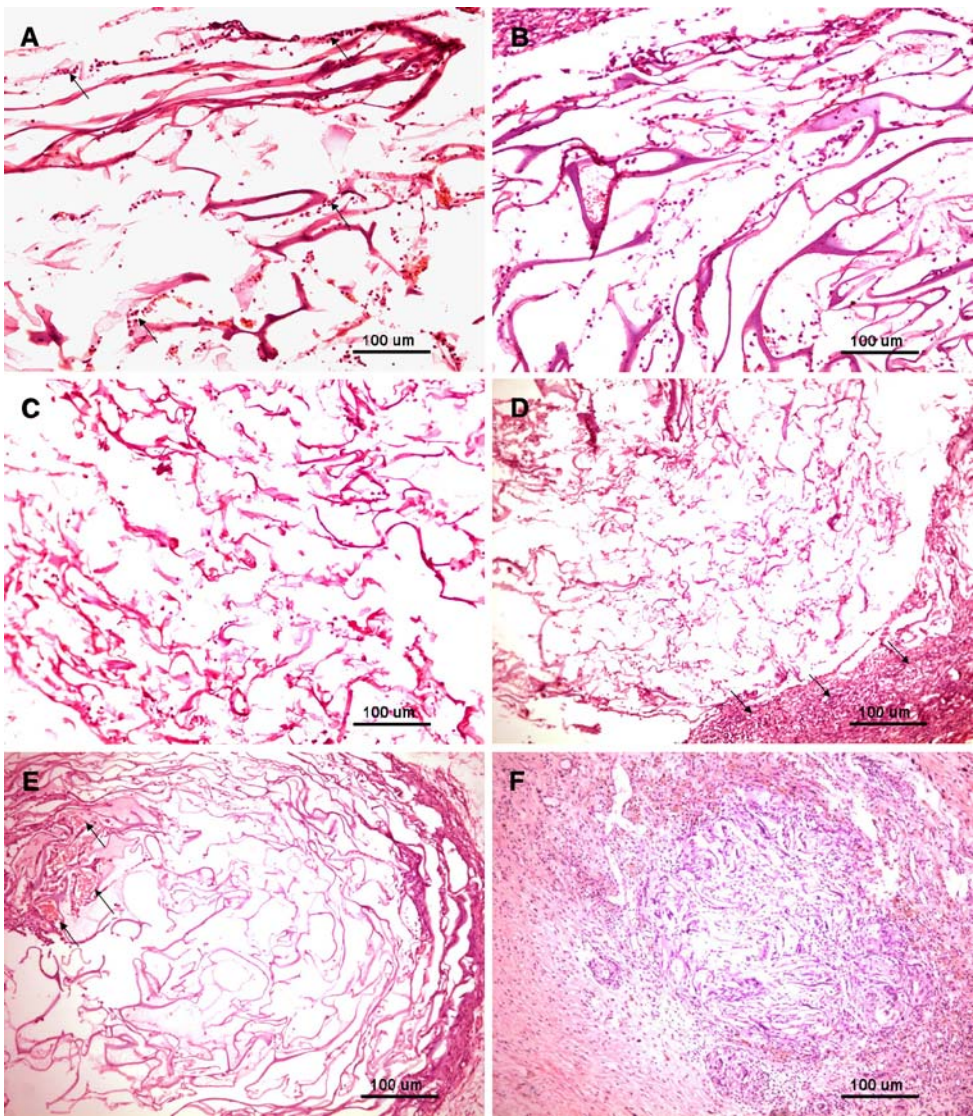

Fig. 5 Degradation of the CII/HyA–CS scaffold and tissue reactions. **a** On day 1, the scaffold was infiltrated by some lymphocytes and neutrophils; the inflammatory cells (*arrows*) were present at the periphery and internal space of the implant (H&E, ×200). **b** On day 3, the inflammatory cell density increased within the implant and in the surrounding connective tissue; (H&E, ×200). **c** On day 7, the number of inflammatory cells had decreased with the scaffold partly degraded (H&E, ×200). **d** On day 14, fibroblasts had arrived from surrounding granulation tissues (*arrows*); degradation of the scaffold continued (H&E, ×200). **e** On day 28, the implant was surrounded and partly replaced by granulation tissues filled with fibroblasts. Some blood vessels (*arrows*) had colonized the granulation tissues (H&E, ×200). **f** On day 84, the scaffold had been totally replaced by vascularized granulation tissues (H&E, ×200)

provided the best microenvironment for ECM production and gene expression of disc cells because the sponge carrier system favored adhesion of cells. Additionally, its porosity may favor diffusion of nutrients and waste products, and may also provide space for new cells and new ECM. Although collagen gels could also support good cell growth, such constructs did not result in either abundant ECM production or ECM gene expression when compared with collagen sponges. Cell growth, ECM production and gene expression in alginate, agarose, and fibrin

Table 2 The production of rat anti-porcine collagen type II antibody (units/ml, average ± s)

Group	1 d	3 d	7 d	14 d	28 d	56 d	84 d
Untreated	1.53 ± 0.24	1.61 ± 0.11	1.67 ± 0.29	1.59 ± 0.51	1.60 ± 0.10	1.64 ± 0.42	1.52 ± 037
Sham-operated	1.71 ± 0.36	1.81 ± 0.22	1.83 ± 0.26	1.53 ± 0.42	1.74 ± 0.40	1.95 ± 0.58	1.89 ± 0.61
Implanted	1.44 ± 0.16	1.85 ± 0.30	1.58 ± 0.21	1.41 ± 0.57	1.96 ± 0.19	1.92 ± 0.32	1.94 ± 0.52

Note: Sera dilution: 1:10, 1 μg = 82 units

microenvironments were inferior. These work suggested that collagen sponge rather than collagen gel may be more suitable as a scaffold for NP tissue engineering because of their porous structure [31].

HyA is an anionic polysaccharide consisting of D-glucuronic acid and *N*-acetyl-D-glucosamine. CII used in this study is positively charged because of its high content of basic amino acid residues such as arginine, lysine, and hydroxylysine. Therefore, CII and HyA have different charges and easily form PIC in an aqueous solution when mixed. PIC formation severely affects the preparation of homogeneous HyA/CII composite matrices. Taguchi et al. found that when the pH value of the CII/HyA solution was maintained at 1–2 or when NaCl solution was added to the CII/HyA solution to a final concentration of 0.4 mol/l, the formation of PIC was effectively suppressed, and the transmittance of the solution was around 80 and 50%, respectively [32]. We improved Taguchi's method; at 4°C, the pH value of the CII solution was adjusted to 1–2 before adding HyA, then the pre-cooled HyA solution was added slowly at a speed of 0.5 ml/min at a ratio of 9:1 (CII:HyA) and at the same time the mixture was kept in stirring condition (300 rpm) at 4°C. After complete mixing, the transmittance detection proved that almost no PIC was formed in this way.

Lyophilization is one of the techniques used in the study of tissue engineered scaffold materials. Here, raw scaffold materials were poured into a mold and quickly frozen to solid phase in a vacuum at −60°C. Then, the surrounding pressure was reduced and enough heat was added to allow the frozen water in the material to sublimate. In this way, the space originally taken up by the water becomes the pore of the scaffold. The size of the pore can be regulated by the pH and the heating rate [33]. On the other hand, the freezing process of the solution before sublimation affects the homogeneity of the pores [34]. In our study, the freezing process for the CII/HyA suspension was performed via the quenching technique, which created a space and time variable of heat transfer throughout the pan, leading to non-uniform nucleation and growth of ice crystals, and ultimately some degree of heterogeneity. In our future work, a constant cooling rate technique will be used for the suspension freezing process to manufacture more uniform porous scaffolds. However, the highly porous 3-dimensional structure of the CII/HyA–CS scaffold allowed not only penetration and proliferation of cells, but also exchange of nutrient and metabolic product. Moreover, it also assures the diffusion of water into the matrix during the stress process. In addition, the scaffold can be manufactured using different molds, which allows generation of specialized shapes.

Tissue-engineered NP scaffolds need to have a certain tension to withstand surgical handling and mechanical loading as well as enough chemical stability to oppose degradation before being replaced by newly synthesized ECM. Since natural CII sponge as a scaffold biomaterial is easily biodegraded, crosslinking within or between the collagen molecules as well as with other elements can enhance the tension and mechanical stability of the collagen fibers. EDC is a compound with active chemical properties that can react with carboxyl groups of aspartic acid and glutamic acid residues, forming an activated but unstable form of O-urea. Pieper et al. had confirmed that NHS effectively increased the number of covalent bonds by forming a more stable ester, raising the denaturation temperature and improving the mechanical properties of the crosslinked scaffold [18]. During the crosslinking process, the system is capable of conjugating 6-CS to either HyA or CII. The resulting material might actually be a random cross conjugation between or within the three components of the scaffold. In addition, unlike the widely used glutaraldehyde crosslinking system, EDC/NHS in our study is not incorporated into the amide cross-links throughout the entire process. This method seems to cause minimal adverse effects to the biocompatibility of our scaffold [18, 35, 36].

Denaturation temperature and collagenase degradation rate are two important indices for evaluating the mechanical stability of scaffolds. These two indices are influenced by the extent of crosslinking and chemical structure of the scaffold [17]. In this study, the increased denaturation temperature and the improved resistance to collagenase enzymatic degradation demonstrated that crosslinked scaffold had better mechanical stability. A net increase in the relative molecular mass of polymers, resulting in an improved degree of tropism and crystallization of the polymers may contribute to increased mechanical stability of the EDC/NHS crosslinked scaffold. On the other hand,

EDC/NHS crosslinking system can also decrease decomposition of polymers by blocking the movement of larger polymeric molecular chains and blocking the penetration of water molecules [37–39]. As we know, sufficient mechanical properties of the constructs are a prerequisite for implants in load bearing areas [40, 41]. Although the increased denaturation temperature and the improved resistance to collagenase enzymatic degradation in the in vitro study suggested higher mechanical stability, further mechanical testing of the scaffold has to be performed in the future as to whether the crosslinked scaffold could meet the mechanical requirement for clinical application.

In this work, preliminary investigation of the cytocompatibility of the CII/HyA–CS scaffold was conducted. Cell proliferation tests showed a good response of NP cells to CII/HyA–CS scaffolds up to 7 days, which was further confirmed by SEM observations. Cell adherence to the scaffold and new pericellular matrix production indicated that CII/HyA–CS scaffolds hold promise for biological cell-material interaction. For histocompatibility and immunogenicity, our results were identical with previous reports that the tissue reaction to implanted collagen material is generally mild [42–44]. Injection or implantation of a biodegradable biomaterial results in an acute inflammation response (i.e. foreign body reaction), mostly followed by more chronic inflammation. These processes generally induce infiltration of inflammatory cells, as well as formation of fibrin, exudates and new blood vessels [45]. These reactions were also observed in our CII/HyA–CS scaffold. In our study, subcutaneous implantation of CII/HyA–CS scaffold resulted in a mild ongoing of foreign body reaction with the number of infiltrated inflammatory cells decreased on day 7, which was in accordance with the inflammatory process caused by surgical trauma. Seven days after surgery, the scaffold had been gradually degraded and replaced by newly-formed granulation tissues. After 3 months, the implant had been totally replaced by granulation tissues and finally assimilated by the host. These data indicate good histocompatibility of the implanted CII/HyA–CS scaffold. Furthermore, as no antibodies to porcine CII were detected in the sera of implanted rats, we conclude that the CII/HyA–CS scaffold also has a low immunogenicity.

In conclusion, We have fabricated a novel scaffold for NP tissue engineering using CII, HyA and 6-CS, the main components of the extracellular matrix of native NP, with techniques of lyophilization and EDC/NHS crosslinking. The fabricated 3D constructs possess similar composition to native NP, have improved mechanical stability, high water-binding capacity and overall high porosity—all of which are critical for NP tissue engineering. In addition, satisfactory biocompatibility and low immunogenicity make the bioactivity of this novel scaffold deserve further investigation. We hope the CII/HyA–CS scaffold can ultimately lead to de novo synthesis of replaced NP by implanting the pre-cultured cell/scaffold hybrids into degenerated IVDs after discectomy.

Acknowledgements This work was supported by the National Natural Science Foundation of China (No. 30772186) and the Youth Science and Research Foundation of the Third Military Medical University (No. XG2005D127).

References

1. Andersson GB, Schultz A, Nathan A, Irstam L. Roentgenographic measurement of lumbar intervertebral disc height. Spine. 1981;6:154–8.
2. Yasuma T, Koh S, Okamura T, Yamauchi Y. Histological changes in aging lumbar intervertebral discs. Their role in protrusions and prolapses. J Bone Joint Surg Am. 1990;72:220–9.
3. Kuslich SD, Ulstrom CL, Michael CJ. The tissue origin of low back pain and sciatica: a report of pain response to tissue stimulation during operations on the lumbar spine using local anesthesia. Orthop Clin North Am. 1991;22:181–7.
4. Schwarzer AC, Aprill CN, Derby R, et al. The prevalence and clinical features of internal disc disruption in patients with chronic low back pain. Spine. 1995;20:1878–83.
5. Hutton WC, Toribatake Y, Elmer WA, et al. The effect of compressive force applied to the intervertebral disc in vivo. A study of proteoglycans and collagen. Spine. 1998;23:2524–37.
6. Lotz JC, Chin JR. Intervertebral disc cell death is dependent on the magnitude and duration of spinal loading. Spine. 2000;25:1477–83.
7. An H, Boden SD, Kang J, et al. Summary statement: emerging techniques for treatment of degenerative lumbar disc disease. Spine. 2003;28:S24–5.
8. Huang RC, Sandhu HS. The current status of lumbar total disc replacement. Orthop Clin North Am. 2004;35:33–42.
9. Inoue H. Three-dimensional architecture of lumbar intervertebral discs. Spine. 1981;6:139–46.
10. Yu J, Winlove CP, Roberts S, Urban JP. Elastic fibre organization in the intervertebral discs of the bovine tail. J Anat. 2002;201:465–75.
11. Paesold G, Nerlich AG, Boos N. Biological treatment strategies for disc degeneration: potentials and shortcomings. Eur Spine J. 2007;16:447–68.
12. Adler JH, Schoenbaum M, Silberberg R. Early onset of disk degeneration and spondylosis in sand rats (*Psammomys obesus*). Vet Pathol. 1983;20:13–22.
13. Wakatsuki T, Elson EL. Reciprocal interactions between cells and extracellular matrix during remodeling of tissue constructs. Biophys Chem. 2003;100:593–605.
14. Yang X, Li X. Nucleus pulposus tissue engineering: a brief review. Eur Spine J. 2009 [Epub ahead of print].
15. Moller HJ, Heinegard D, Poulsen JH. Combined alcian blue and silver staining of subnanogram quantities of proteoglycans and glycosaminoglycans in sodium dodecyl sulfate-polyacrylamide gels. Anal Biochem. 1993;209:169–75.
16. Zhang R, Ma PX. Porous poly(L-lactic acid)/apatite composites created by biomimetic process. J Biomed Mater Res. 1999;45:285–93.
17. Liu LS, Thompson AY, Heidaran MA, et al. An osteoconductive collagen/hyaluronate matrix for bone regeneration. Biomaterials. 1999;20:1097–108.
18. Pieper JS, Hafmans T, Veerkamp JH, et al. Development of tailor-made collagen–glycosaminoglycan matrices: EDC/NHS

crosslinking, and ultrastructural aspects. Biomaterials. 2000; 21:581–93.
19. Rong Y, Sugumaran G, Silbert JE, et al. Proteoglycans synthesized by canine intervertebral disc cells grown in a type I collagen–glycosaminoglycan matrix. Tissue Eng. 2002;8:1037–47.
20. Sato M, Kikuchi M, Ishihara M, et al. Tissue engineering of the intervertebral disc with cultured annulus fibrosus cells using atelocollagen honeycomb-shaped scaffold with a membrane seal (ACHMS scaffold). Med Biol Eng Comput. 2003;41:365–71.
21. Brown RQ, Mount A, Burg KJ. Evaluation of polymer scaffolds to be used in a composite injectable system for intervertebral disc tissue engineering. J Biomed Mater Res A. 2005;74:32–9.
22. Seguin CA, Grynpas MD, Pilliar RM, et al. Tissue engineered nucleus pulposus tissue formed on a porous calcium polyphosphate substrate. Spine. 2004;29:1299–306; discussion 1306–1297.
23. Chiba K, Andersson GB, Masuda K, et al. Metabolism of the extracellular matrix formed by intervertebral disc cells cultured in alginate. Spine. 1997;22:2885–93.
24. Baer AE, Wang JY, Kraus VB, et al. Collagen gene expression and mechanical properties of intervertebral disc cell-alginate cultures. J Orthop Res. 2001;19:2–10.
25. Le Visage C, Yang SH, Kadakia L, et al. Small intestinal submucosa as a potential bioscaffold for intervertebral disc regeneration. Spine. 2006;31:2423–30; discussion 2431.
26. Crevensten G, Walsh AJ, Ananthakrishnan D, et al. Intervertebral disc cell therapy for regeneration: mesenchymal stem cell implantation in rat intervertebral discs. Ann Biomed Eng. 2004;32:430–4.
27. Roughley P, Hoemann C, DesRosiers E, et al. The potential of chitosan-based gels containing intervertebral disc cells for nucleus pulposus supplementation. Biomaterials. 2006;27:388–96.
28. Yang SH, Chen PQ, Chen YF, et al. An in vitro study on regeneration of human nucleus pulposus by using gelatin/chondroitin-6-sulfate/hyaluronan tri-copolymer scaffold. Artif Organs. 2005;29:806–14.
29. Sakai D, Mochida J, Iwashina T, et al. Atelocollagen for culture of human nucleus pulposus cells forming nucleus pulposus-like tissue in vitro: influence on the proliferation and proteoglycan production of HNPSV-1 cells. Biomaterials. 2006;27:346–53.
30. Halloran DO, Grad S, Stoddart M, et al. An injectable crosslinked scaffold for nucleus pulposus regeneration. Biomaterials. 2008;29:438–47.
31. Gruber HE, Leslie K, Ingram J, et al. Cell-based tissue engineering for the intervertebral disc: in vitro studies of human disc cell gene expression and matrix production within selected cell carriers. Spine J. 2004;4:44–55.
32. Taguchi T, Ikoma T, Tanaka J. An improved method to prepare hyaluronic acid and type II collagen composite matrices. J Biomed Mater Res. 2002;61:330–6.
33. Doillon CJ, Whyne CF, Brandwein S, et al. Collagen-based wound dressings: control of the pore structure and morphology. J Biomed Mater Res. 1986;20:1219–28.
34. O'Brien FJ, Harley BA, Yannas IV, et al. Influence of freezing rate on pore structure in freeze-dried collagen–GAG scaffolds. Biomaterials. 2004;25:1077–86.
35. Charulatha V, Rajaram A. Influence of different crosslinking treatments on the physical properties of collagen membranes. Biomaterials. 2003;24:759–67.
36. Lee CR, Grodzinsky AJ, Spector M. The effects of cross-linking of collagen–glycosaminoglycan scaffolds on compressive stiffness, chondrocyte-mediated contraction, proliferation and biosynthesis. Biomaterials. 2001;22:3145–54.
37. Cao H, Xu S-Y. EDC/NHS-crosslinked type II collagen–chondroitin sulfate scaffold: characterization and in vitro evaluation. J Mater Sci: Mater Med. 2008;19:567–75.
38. Hutmacher DW. Scaffolds in tissue engineering bone and cartilage. Biomaterials. 2000;21:2529–43.
39. Pieper JS, van der Kraan PM, Hafmans T, et al. Crosslinked type II collagen matrices: preparation, characterization, and potential for cartilage engineering. Biomaterials. 2002;23:3183–92.
40. Hunziker EB. Articular cartilage repair: basic science and clinical progress. A review of the current status and prospects. Osteoarthritis Cartilage. 2002;10:432–63.
41. Al-Munajjed AA, Hien M, Kujat R, et al. Influence of pore size on tensile strength, permeability and porosity of hyaluronan–collagen scaffolds. J Mater Sci: Mater Med. 2008;19:2859–64.
42. Anselme K, Bacques C, Charriere G, et al. Tissue reaction to subcutaneous implantation of a collagen sponge. A histological, ultrastructural, and immunological study. J Biomed Mater Res. 1990;24:689–703.
43. van Wachem PB, Plantinga JA, Wissink MJ, et al. In vivo biocompatibility of carbodiimide-crosslinked collagen matrices: effects of crosslink density, heparin immobilization, and bFGF loading. J Biomed Mater Res. 2001;55:368–78.
44. Gagnieu CH, Forest PO. In vivo biodegradability and biocompatibility of porcine type I atelocollagen newly crosslinked by oxidized glycogen. Biomed Mater Eng. 2007;17:9–18.
45. Anderson JM, Shive MS. Biodegradation and biocompatibility of PLA and PLGA microspheres. Adv Drug Deliv Rev. 1997;28: 5–24.